Polymer Bulletin (2021) 78:833–848
https://doi.org/10.1007/s00289-020-03137-z

ORIGINAL PAPER

Thermo-mechanical and antimicrobial properties of natural rubber-based polyurethane nanocomposites for biomedical applications

Ekasit Anancharoenwong[1] · Wannarat Chueangchayaphan[1] · Natthida Rakkapao[1,2] · Sutida Marthosa[1,2] · Boonphop Chaisrikhwun[1]

Received: 24 October 2019 / Revised: 13 February 2020 / Accepted: 23 February 2020 /
Published online: 27 February 2020

Abstract

A polyester-type polyurethane (PU) was prepared using hydroxyl-terminated natural rubber (HTNR) as the soft polymer segments, 4,4-methylene dicyclohexyl diisocyanate (H_{12}MDI) as the hard segments and 1,4-butane diol (BDO) as a chain extender. A simple one-shot bulk polymerization method using tetrahydrofuran (THF) as the solvent was chosen. The molar ratio of (H_{12}MDI:HTNR:BDO) was fixed at 1.05:0.5:0.5. The pristine PU and its composite films with titanium nanoparticles (TiO_2), silver nanoparticles (AgNPs) and benzoic acid (BA) were prepared with a constant 0.5 wt% loading of the antimicrobial fillers. The pristine PU and PU composite films were obtained by solution casting and drying at 60 °C in a vacuum oven. The effects of the antimicrobial fillers on the physical structure, mechanical properties, thermal properties, and antimicrobial activities were investigated. The SEM images showed that TiO_2 and AgNPs aggregated. The aggregates reduced the films' tensile strength as they obstructed the transfer of mechanical loads from PU matrix to the dispersed fillers. In contrast, BA was clearly well dispersed in the matrix giving much better mechanical properties (12 MPa tensile strength and 278% strain at break) and the PU–BA films were transparent. The PU–BA composites appear promising for biomedical applications.

✉ Ekasit Anancharoenwong
ekasit.a@psu.ac.th

[1] Faculty of Science and Industrial Technology, Prince of Songkla University, Surat Thani Campus, Surat Thani 84000, Thailand

[2] Center of Excellence in Membrane Science and Technology, Faculty of Science, Prince of Songkla University, Hat Yai Campus, Songkhla 90112, Thailand

Graphic abstract

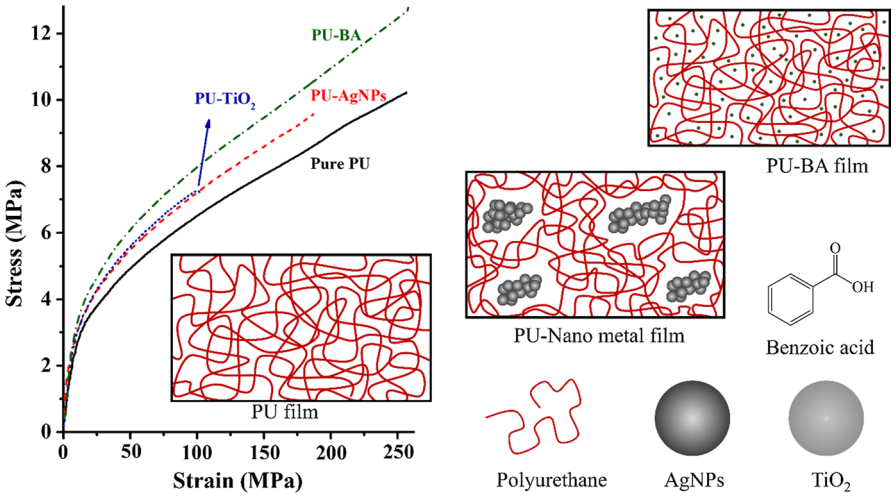

Keywords Antimicrobial film · Polyurethane · Hydroxyl-terminated natural rubber

Introduction

Synthetic and natural polymers are extensively used in medical applications. Several biodegradable polymers based on polyurethane, such as hydroxyl-terminated natural rubber (HTNR), chitosan, collagen, poly (caprolactone) (PCL), poly (ethylene glycol) (PEG), poly (propylene glycol) (PPG) and poly (ester urethane) [1], have been widely used. Among them, HTNR exhibits attractive properties and has been used as the soft segments that provide flexibility and durability to the final polyurethane materials.

Natural rubber (NR) is a renewable polymer, and it has been used to prepare telechelic liquid natural rubber (TLNR). Such modified NR can replace other polymers including petroleum-based elastomers, waterborne polyurethane, photo-cured polyurethane and polyurethane. Theoretically, there are many telechelic NR preparation methods, such as redox method, ozonolysis oxidation, oxidation at high temperature and pressure, photochemical method, metathesis reaction and chemical oxidation. Chemical oxidation was chosen in this work to produce HTNR because of its high selectivity and repeatability [2]. HTNR was then used to form embedded polyurethane (PU) materials, which are most popular in medical applications due to good biocompatibility and adjustable mechanical properties [3].

Three embedded antimicrobial materials were considered in this work: silver nanoparticles (AgNPs), titanium nanoparticles (TiO_2) and benzoic acid (BA). Silver nanoparticles have found applications in various fields such as optics [4], electronics [5], medicine [6], nanomedicine [7] and pharmacy [8]. Especially,

AgNPs have been employed in wound dressings [9] owing to their excellent bactericidal activity against both gram-positive and gram-negative bacteria and against multidrug resistant strains. Note that the silver concentration is an important factor because the release rate of silver depends on its properties and its concentration in the polymer matrix [10].

Comparatively, titanium nanoparticles (TiO_2) have also shown great interfacial properties in the regeneration of hard tissues, good corrosion resistance, lack of inflammatory responses, cell viability and strong antimicrobial activity under UV light.

Another interesting antimicrobial filler is benzoic acid (BA). It is a natural acid from plants, and it is widely used as a food preservative. BA is relatively nontoxic. It inhibits the growth of mold, yeasts and bacteria. It can be excreted as hippuric acid from human body; thus, it is suitable for medical applications. However, only a few studies have reported the use of benzoic acid in biomaterials, for antibacterial activity. This work was, therefore, designed to explore this interesting knowledge gap.

In this work, *cis*-1,4 polyisoprene-based PU films of a new type were prepared by a simple one-step method [11], with three alternative antimicrobial fillers: silver nanoparticles (AgNPs), titanium nanoparticles (TiO_2) and benzoic acid (BA) at 0.5 wt% based on polyurethane. The study aimed to improve both mechanical and antimicrobial properties of the new polyurethane nanocomposites. The study explored the morphological, chemical and antimicrobial activities including tensile testing, thermogravimetric analysis and dynamic mechanical analysis of the composite films.

Materials and methods

Materials

4,4′-dicyclohexylmethane diisocyanate (H_{12}MDI) was procured from Sigma-Aldrich, Germany. Hydroxyl-terminated natural rubber (HTNR) with an average molecular weight of 1000 was prepared in the laboratory by the chemical degradation of natural rubber [12]. Dibutyltin dilaurate (DBTL, 95%, Sigma-Aldrich, Germany) and nitrogen gas (99.999%, Kuang Li Oxygen Co., Ltd.) were purchased. The AgNPs were prepared in-house by using silver nitrate salt ($AgNO_3$) and tannic acid as a reducing agent. The AgNP particle size was approximately 10 nm in diameter. BA was purchased from Kemaus (Australia), and TiO_2 (21 nm) was procured from Sigma-Aldrich (America).

Methods

The sample preparation and characterization methods are described in this section.

Sample preparation

PU and PU composites were synthesized by a one-shot method in a three-neck round bottom flask equipped with a distillation bridge and N_2 gas inlet. The HTNR acted as a polyol, and the 1,4-butanediol (BDO) acted as a chain extender, while H_{12}MDI was used as the diisocyanate. Firstly, 4.84 g of HTNR and 0.44 g of chain extender were dissolved in THF. Then, 0.04 g of catalyst DBTL was added to the solution, followed by the dropwise addition of 2.66 g of H_{12}MDI. The reaction temperature was kept at 60 °C for 3 h. The obtained mixture was poured into a glass mold and heated continuously in an oven at 60 °C for 48 h to produce a polyurethane sheet. The average film thickness was 0.3–0.5 mm. The molar ratio of H_{12}MDI:HTNR:BDO was 1.05:0.5:0.5 with 41.3% and 58.7% proportions of the hard and the soft segments.

Suspension of AgNPs in water was prepared using a chemical reduction method. Before use, all glassware was cleaned in a bath of aqua regia solution and rinsed thoroughly with deionized water. The syntheses were carried out using the constant 1:2 molar ratio of silver nitrate to tannic acid at 100 °C. Silver nitrate suspension was first heated to its boiling point under reflux, and then, a mixture of tannic acid was introduced to the reaction mixture. The solution was heated for an additional 15 min and cooled to room temperature [13]. The concentration of silver ions in all solutions was 100 ppm.

To prepare the PU–AgNPs, PU–TiO_2 and PU–BA films, the starting polyurethane solution was prepared as described, and then, 0.5 wt% of each antimicrobial substrate was added to the PU solution for composite preparation. The mixture was continuously stirred for 10 min, sonicated for 10 min, poured into glass molds and heated in an oven at 60 °C for 48 h to produce the filled PU composite sheets.

Characterization

1. Water contact angle

Water contact angles on the film's top surface were measured using a contact angle meter (OCA 15 EC, Data Physics, Germany). The water droplet size for the measurements was approximately 10 µL. The contact angles were measured at five different points, and the average values are reported.

2. Tensile testing

The film specimens were die-cut from PU sheets with die type 5A according to ISO 527. The tensile properties were determined according to ASTM D412 standard with a universal tensile testing machine (Tinius Olsen, model 10ST, Salford, England) at a cross-head speed of 200 mm min^{-1}. Three specimens were tested for each sample type, and the average and standard deviation are reported. The Young's modulus was determined as the initial slope of the stress–strain curve.

3. Antimicrobial activity

To test the antimicrobial efficiencies of the PU composites, the following test organisms were used: *Pseudomonas aeruginosa* (*P. aeruginosa*) and *Staphylococcus aureus* (*S. aureus*), which represent gram-negative and gram-positive bacteria, respectively. *P. aeruginosa* infections are serious problems in patients hospitalized with cancer, cystic fibrosis or burns, with high fatality rates. *Pseudomonas aeruginosa* is naturally resistant to a wide range of antibiotics. *S. aureus* is a pathogenic microorganism causing many diseases such as toxic shock syndrome, superficial skin lesions and deep-seated infections. It is the leading overall cause of hospital-acquired (nosocomial) infections of surgical wounds. Moreover, it is resistant to a great number of antimicrobial agents.

Pseudomonas aeruginosa and *S. aureus* are considered common potential pathogens for infections, so they were selected for the evaluation of the antimicrobial efficiency in this study. Percent reduction of organisms (*R*%), which indicates biostatic efficiency from contact with the samples, was determined using the following formula:

$$R(\%) = \frac{B - A}{B} \times 100 \tag{1}$$

where A is the CFU per milliliter of the medium with the treated substrate after incubation and B is the CFU per milliliter of the medium in the control samples after incubation.

Colony-forming units To determine the antibacterial activities, two types of microorganisms (gram-negative *P. aeruginosa* bacteria and gram-positive *S. aureus* bacteria) were suspended to the final density of 1×10^8 CFU/mL in phosphate-buffered saline (PBS) according to 0.5 McFarland turbidity standard (approximately $1–2 \times 10^8$ CFU/mL). In order to obtain colony counts, tenfold dilution was performed to obtain the final density of 1×10^7 CFU/mL in nutrient broth.

Film samples were cut into 5 mm in diameter. Total weight of 0.3 g was sterilized with UV light for 30 min before immersion in 5 mL of the bacterial suspension in a 50-mL conical tube. The media were shaken at 200 rpm at 37 °C for 30, 60, 90 and 120 min. After the shaking incubation, 100 µL of the culture was spread over an entire agar plate. Thereafter, the plates were incubated at 37 °C overnight and CFU/mL was counted.

4. Scanning electron microscopy

A scanning electron microscope (SEM, FEI Quanta 400, JEOL Ltd., Tokyo, Japan) was used for a morphological characterization of the films. The sample films were cryogenically fractured in liquid nitrogen to prepare a fresh cross section prior to drying. The dried samples were gold-coated and then imaged using the SEM.

5. Dynamic mechanical analysis

The PU and PU composites were subjected to dynamic mechanical analysis (DMA) using a PerkinElmer DMA 8000 (PerkinElmer Inc., Waltham, USA) in the temperature/time scan mode. The temperature range of − 100 to 100 °C was covered with the heating rate of 2 °C min^{-1}, and frequency was set at 1 Hz. The storage and loss moduli were determined.

6. Fourier transform infrared spectroscopy

The FTIR spectra of PU, PU–AgNPs, PU–TiO_2 and PU–BA films were measured using a PerkinElmer Spectrum II FTIR Spectrometer (USA) equipped with a universal attenuated total reflectance sensor (UATR) sampling accessory. Note that only the top surface of the sample films was analyzed, in order to avoid the influence of the inorganic particle agglomerates on the spectra. The FTIR spectra were collected at room temperature using UATR mode in the range of 4000–400 cm^{-1} with 32 scans per spectrum at a resolution of 2 cm^{-1}.

7. Thermogravimetric analysis

Thermogravimetric analysis (TGA) of the polyurethane films was done using a TG/DSC + thermo-analyzer from Mettler Toledo. Measurements were taken over the temperature range of 30–800 °C, at a constant the heating rate of 10 °C min^{-1} in nitrogen, and the initial sample mass was approximately 10 mg. Based on the TG curves, temperatures corresponding to mass losses of 1, 5, 10 and 50% are reported.

Results and discussion

Morphological characterization

Morphology study of the film's cross sections from the cryo-fractured PU composite films showed different compatibilities of the antimicrobial fillers with the polyurethane matrix. Morphologies of samples from the top and bottom parts of each film were distinguished, and cross-sectional images of both were analyzed. Morphology was expected to affect the mechanical properties the film composites.

Figure 1 shows the SEM cross-sectional images of the polyurethane composites with TiO_2, AgNPs and BA. Figure 1a–d shows the cross-sectional images of materials on the top part of PU, PU–TiO_2, PU–AgNPs and PU–BA films. Figure 1e–j presents the cross-sectional images of the bottom parts of PU, PU–TiO_2, PU–AgNPs and PU–BA films. The top parts did not show significant numbers of particles in any of the samples (Fig. 1a–d), while the bottom parts exhibited particles (Fig. 1e–h).

As clearly seen in Fig. 1h, the PU–BA films displayed nearly similar morphology to the pure PU in Fig. 1e, while PU–TiO_2 and PU–AgNPs in Fig. 1f and g appeared to have micro-agglomerates at the bottom. This indicates that the inorganic fillers

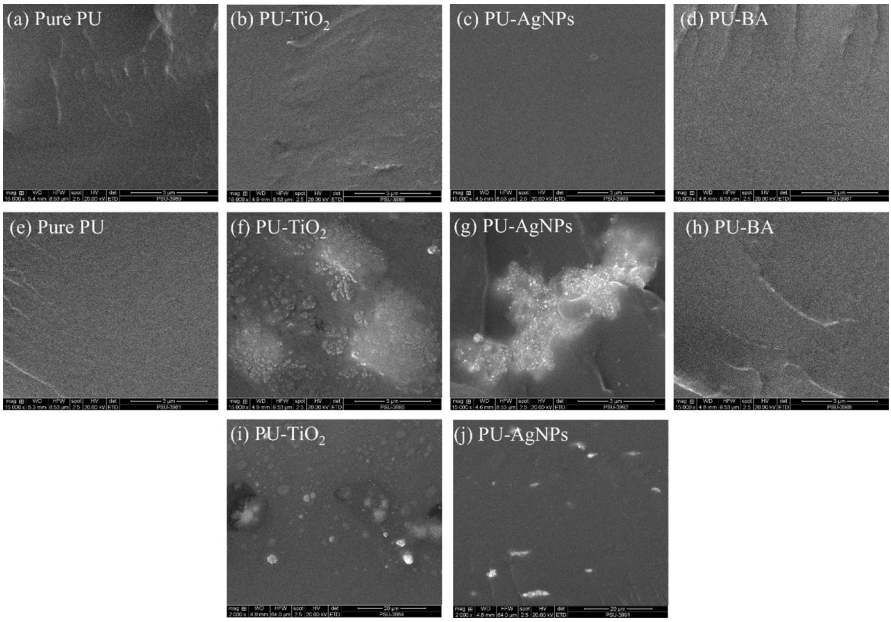

Fig. 1 Cross-sectional SEM images of PU and PU composite films; **a**–**d** materials from the top part at ×15,000 magnification, **e**–**h** materials from the bottom part at ×15,000 magnification, **i** and **j** materials from the bottom part at ×2000 magnification

(TiO_2 and AgNPs) were poorly dispersed in the matrix. The nanoparticles aggregated and formed clusters in the films at the bottom of PU matrix, observable at 2000× magnification (Fig. 1i, j). The agglomeration was expected to reduce tensile strength of PU–TiO_2 and PU–AgNPs films. The mechanical results indeed show reduced tensile strength and elongation at break for both PU–TiO_2 and PU–AgNPs films, which can be explained by incompatibility and poor interfacial adhesion between the fillers and the PU matrix [14]. Inorganic TiO_2 and AgNPs are relatively hydrophilic, while the polyurethane matrix of hydroxyl-terminated natural rubber is hydrophobic, so that poor interfacial adhesion due to this incompatibility could lead to the poor dispersion and agglomeration of TiO_2 and AgNPs in the PU matrix [15] as seen in Fig. 1.

In contrast, the organic filler BA had a different impact on the film morphology when compared to TiO_2 and AgNPs. PU–BA films had similar morphology to the pure PU film. BA could disperse well in PU matrix as these were compatible. This compatibility was induced by hydrogen bonding between carbonyl groups on BA with urethane groups in the polyurethane. This morphology finding agrees well with the mechanical observations (tensile strength and elongation at break) of the PU–BA film.

Apart from the morphology, film color and appearance are also important practical aspects and they were observed. PU–AgNPs films were dark, PU–TiO_2 films were opaque, and PU–BA films were transparent.

Wettability

The water contact angle (WCA) of the film is the angle between the film's surface and the tangent line at the contact point with a water droplet on the surface. It quantifies the wettability of the film surface and is used as an indicator of the relative hydrophilicity. A low contact angle indicates relatively good wetting and hydrophilicity properties [16].

The water contact angles of the prepared PU and PU composite films are shown in Fig. 2. The average 127.4° WCA of the pure PU film was the highest, while the PU–TiO_2, PU–AgNPs and PU–BA had 90.7°, 83.6° and 68.0°, respectively. The results indicate that the incorporation of the antimicrobial fillers enhanced hydrophilicity of the films, and this was caused by the hydrophilic properties of TiO_2 [17], AgNPs [18] and BA [19]. Although hydrophilicity reduces the water resistance of the PU composite films, it favorably facilitates the antimicrobial activity by improving the contact of microbial cells with the film [7, 20].

Mechanical properties

The mechanical properties, tensile strength, elastic modulus and elongation at break, of the PU and PU composite films were investigated by tensile testing at room temperature. The stress–strain curves of the PU films are shown in Fig. 3a, and their slopes are positive, indicating that the films behave as thermoplastic elastomers. All the composite films clearly exhibited higher stress–strain curves than the pure PU films. This indicates that the incorporation of these fillers tended to improve the stress–strain behavior, and they acted as reinforcing fillers. This result correlates well with the increased interaction between PU matrix and filler as shown in FTIR results (Fig. 4). From Fig. 3a, the stress–strain curve for PU–BA film was

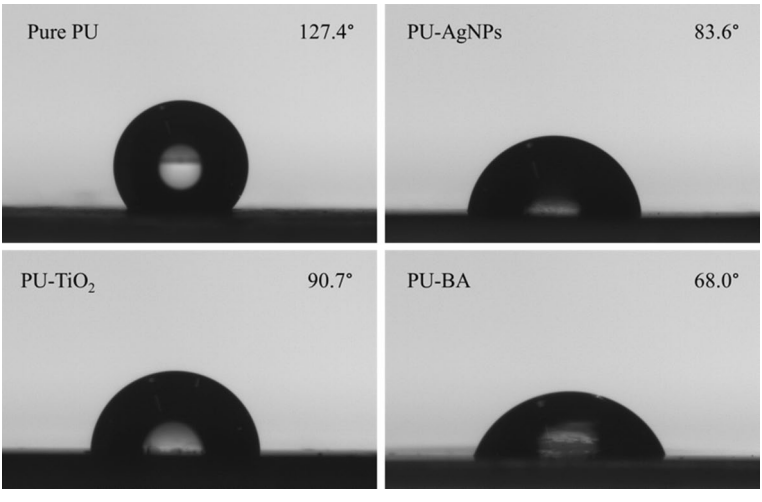

Fig. 2 Water contact angles of PU and PU composites with TiO_2, AgNPs and BA

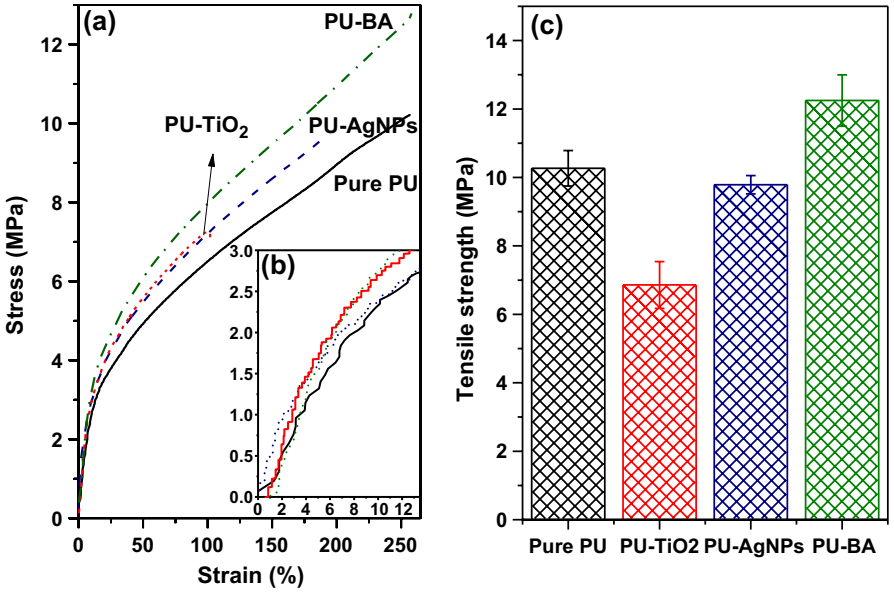

Fig. 3 **a** Stress versus strain curves, **b** initial stress strain curves and **c** tensile strength of the PU and PU composite films filled with TiO_2, AgNPs and BA

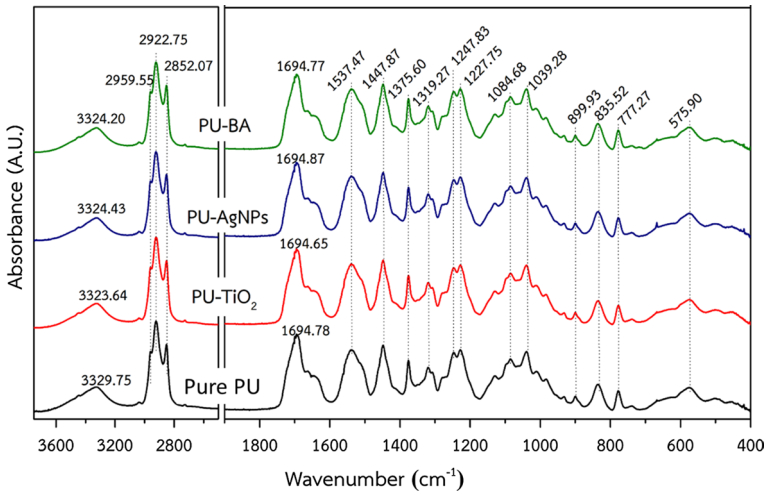

Fig. 4 FTIR spectra of PU and PU composites with TiO_2, AgNPs and BA

the highest, while those for PU–TiO_2 and PU–AgNPs films were below this one. PU–TiO_2 and PU–AgNPs films incorporated inorganic fillers which aggregated and formed micro-phase separation, leading to the lower stress–strain curves when

compared to that for the PU–BA film which had no micro-phase separation of organic BA within the films (Fig. 1).

Furthermore, Fig. 3a reveals that the fillers affected the elongation at break of the films. The elongations at break were 253%, 110%, 160% and 260% for PU, PU–TiO_2, PU–AgNPs and PU–BA, respectively. The inorganic fillers (TiO_2 and AgNPs) gave lower elongations than the pure PU film. This poor mechanical performance was due to the aggregation of inorganic fillers in PU matrix, as seen in Fig. 1. Young's modulus was determined from the initial slope of the stress–strain curves. The inset of Fig. 3b shows insignificant differences in the initial stress–strain curves so it was concluded that the Young's modulus of the pure PU and PU composites did not significantly differ.

Referring to Fig. 3c, the tensile strength was 10.2, 6.8, 9.7 and 12.2 MPa for pure PU, PU–TiO_2, PU–AgNPs and PU–BA, respectively. The tensile strength of PU–TiO_2 and PU–AgNPs was lower than that of pure PU film because of the poor compatibility of TiO_2 and AgNPs with PU matrix effectively restricting mobility of PU chains in the film [21]. On the other hand, the organic BA filler was molecularly compatible with PU, so it delivered homogenous PU–BA composite films with strong hydrogen bonding between PU and BA [22]. Thus, PU–BA film showed the highest tensile strength with an improved elongation at break (260%) when compared to the pure PU film (253%). Overall, the PU–BA film had superior mechanical properties when compared to others in this study.

Fourier transform infrared spectroscopy

FTIR spectroscopy was employed to characterize the chemical interactions between the fillers and PU matrix, and the results are presented in Fig. 4. In order to avoid the influence of agglomerates of the inorganic particles (Fig. 1), only the top surfaces were analyzed.

The PU film showed N–H stretching vibrations of the hydrogen-bonded amine groups at 3331–3323 cm^{-1} and showed the characteristic C=O stretching vibrations of the hydrogen-bonded urethane carbonyl groups at 1694 cm^{-1} [23, 24]. FTIR spectra for all the composite films contained an N–H band at 3331–3323 cm^{-1} which shifted to lower wavenumbers (red shift), while C=O stretching vibrations at 1694 cm^{-1} were unchanged by the fillers. This phenomenon indicates that interactions between the antimicrobial fillers and PU were significant at the N–H groups of PU, while the C=O groups showed less activity.

Referring to the SEM images, the PU–BA and pure PU films had good homogeneity indicating compatibility at the molecular level, associated with strong hydrogen bonding between the carboxylic group of BA and amine groups of PU [22]. This molecular compatibility improved the mechanical properties of the composite PU–BA compared to the pure PU film.

On the other hand, the SEM images of PU–AgNPs and PU–TiO_2 films show micro-phase separation due to agglomeration of the inorganic fillers at the bottom side of the films due to particle settling in gravity. The poor compatibility between the PU and filler had weaker interfacial interactions between particles and PU and

suppressed the mechanical properties of the composites, PU–AgNPs and PU–TiO_2, compared to the pure PU film.

Thermogravimetric analysis

The TGA–DTG curves of HTNR-based PU in nitrogen gas with the heating rate of 10 °C min^{-1} are shown in Fig. 5. The thermogravimetric analysis (TGA) of pristine PU and PU composites shows three significant stages labeled (I), (II) and (III) in Fig. 5. Firstly, a small weight loss corresponding to evaporation of THF and some other small molecules can be observed between 80 and 150 °C. Then, the first stage (I) was accompanied by mass loss in the temperature range 318–361 °C, corresponding to the depolymerization of PU, as the urethane groups broke up into isocyanates and polyols. The isocyanate segments formed from decomposition could not volatilize and were trapped in the residues [1, 25, 26]. Then, in the second stage (II), the polyol segments started to decompose into some aliphatic ether alcohols as the temperature increased in 340–384 °C [26]. The products became more complex with increasing temperature, and even epoxy compounds were formed by chemical interactions. Stage (III) was in the temperature range 426–436 °C, where the materials decomposed into primary amines, secondary amines, vinyl ethers and CO_2. When the temperature rose to 500 °C, the whole thermal degradation process was almost finished. This stage was associated with the thermal stability of pristine PU and the PU composite films [26].

Figure 5 shows TGA–DTG thermograms of the films up to 550 °C. Thermograms of the composite films are shifted toward lower temperatures in comparison with the pure PU. In all stages, the composite films began to degrade at a lower temperature than the pure PU film, so Fig. 5 indicates that the antimicrobial filler addition

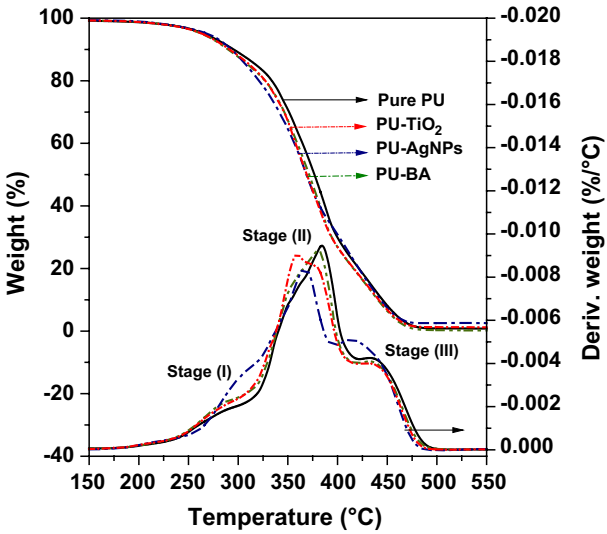

Fig. 5 TGA–DTG thermograms of pristine PU and PU composites with TiO_2, AgNPs and BA

degraded the thermal stability of the films. Thermal degradation was the strongest with AgNPs filler [especially in stages (I) and (III)], and TiO_2 was moderate, while BA was the lowest. The impact of thermal degradation is explained by thermal properties of these fillers. The specific heat capacities of AgNPs and TiO_2 are 24.9 J mol^{-1} K^{-1} [27] and 55.10 J mol^{-1} K^{-1} [28], respectively. AgNPs have lower specific heat capacity, and it conducted more heat to the PU matrix than TiO_2 so PU–AgNPs film began to degrade at a lower temperature than PU–TiO_2, as shown in Fig. 5. In conclusion, filler with a low specific heat capacity could facilitate thermal degradation of the PU composite film.

Dynamic mechanical thermal analysis

It is well recognized that the storage modulus of a particulate-filled polymer composite is influenced by the effective interfacial interactions between the filler particles and the polymer matrix. In general, strong interfacial interactions between the matrix and the filler improve storage modulus of the composite [29]. Dynamic mechanical thermal analysis (DMTA) was exploited to characterize the interfacial interactions between the filler and the PU matrix. The storage modulus and the loss modulus of the pure PU and PU composites with TiO_2, AgNPs and BA are shown in Fig. 6.

It is clearly observed that the PU–BA film had a greater storage modulus than the pure PU, PU–AgNPs or PU–TiO_2, where AgNPs and TiO_2 are inorganic fillers. The high storage modulus might be due to the strong H-bonding between BA and

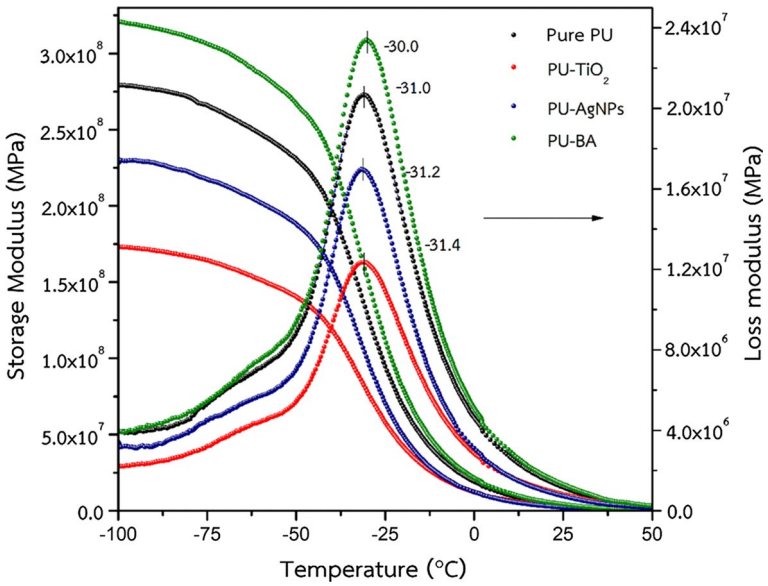

Fig. 6 The storage modulus and loss modulus plotted as functions of temperature for PU and PU composite films

PU matrix in the PU–BA films. The H-bonding interactions could restrict molecular mobility, effectively promoting storage modulus, and reflected in the high glass transition temperature (Tg) of the composite PU–BA, when compared to pure PU.

Different phenomena occurred in the PU composites with the inorganic, AgNPs and TiO_2, fillers. The micro-phase separation due to agglomeration of the inorganic fillers in the PU matrix lowered the storage modulus and Tg of these composites in comparison with the pure PU film. This could be explained by the weaker interactions between the inorganic fillers and the urethane groups of PU chains, also suppressing the thermal–mechanical properties of PU–AgNPs and PU–TiO_2 when compared to the pure PU film.

Antimicrobial activity

The antimicrobial properties of the samples were tested against *P. aeruginosa* and *S. aureus*. The pure PU film without antimicrobial activity was used as a control. Antimicrobial capabilities of the PU composites with 0.5 wt%. fillers are shown in Fig. 7. All the PU composites exhibited antimicrobial activity against *S. aureus,* especially PU–AgNPs that caused *S. aureus* reduction by more than 99%. Clearly, the growth of *S. aureus* microorganisms in the medium was affected by the presence of AgNPs [30]. On the other hand, PU–TiO_2 and PU–BA showed lesser efficacy against *S. aureus*, with only 19 and 32% bacterial reductions, respectively. The low bacterial reduction of PU–TiO_2 might be due to the lack of UV light in the experiment, so TiO_2 might not have been at its full capacity. Noticeably, all the PU composite films had higher efficiency against *S. aureus* than against *P. aeruginosa.* The complicated cell walls of *P. aeruginosa* may have reduced activity of the antimicrobial substrates acting on bacterial cells, leading to the low bacterial reduction. Gram-negative bacteria are known to be resistant to most of the antimicrobial material due to their

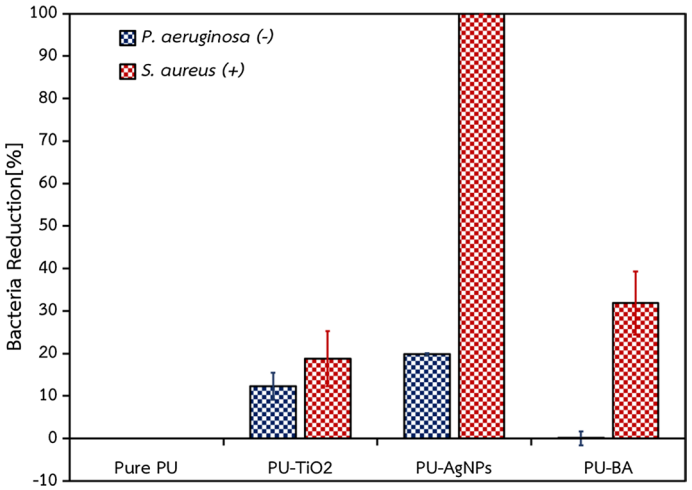

Fig. 7 Antimicrobial activities of the PU and composite PU films against *S. aureus* and *P. aeruginosa*

outer membrane which contains the structural lipopolysaccharide components, making their cell wall impermeable to antimicrobial fillers [31].

Conclusion

Hydroxyl-terminated natural rubber was used to synthesize polyurethane composites which were filled with TiO_2, AgNPs or BA. SEM images confirmed the agglomeration of filler particles in PU–TiO_2 and PU–AgNPs composites. The agglomerates reduced filler–polymer interfacial area, formed micro-phase separation and decreased both tensile strength and storage modulus of PU–TiO_2 and PU–AgNPs films. In contrast, the PU–BA film showed homogeneously dispersed filler that was molecularly miscible in the PU matrix, giving film that was transparent, had good mechanical properties (increased Tg and energy adsorption) and higher storage modulus in comparison with others.

The tested antimicrobial fillers in PU matrix reduced the thermal stability of PU. The fillers improved heat transfer as the temperature was raised, thereby increased thermal degradation of the composites. On the other hand, the water contact angles indicated that the antimicrobial fillers enhanced hydrophilicity of PU, especially in the PU–BA sample, which could be beneficial when in contact with microbial cells.

The PU–BA transparent film, which had the highest tensile strength, elongation at break and storage modulus, is suitable for biomedical application emphasizing mechanical properties, but it is only effective toward *S. aureus* reduction. Although the PU–AgNPs sample exhibited the strongest antimicrobial activity, it was dark and had an unattractive appearance.

Acknowledgements We are grateful to the Faculty of Science and Industrial Technology for the use of their laboratory facilities and to Assoc. Prof. Dr. Seppo Karrila for reviewing the manuscript. This work was supported by the government budget (or budget revenue) of Prince of Songkla University year 2015, Grant No. SIT590171d.

References

1. Filip D, Macocinschi D, Vlad S (2011) Thermogravimetric study for polyurethane materials for biomedical applications. Compos Part B Eng 42(6):1474–1479. https://doi.org/10.1016/j.compositesb-2011.04.050
2. Phinyocheep P, Phetphaisit C, Derouet D, Campistron I, Brosse J (2005) Chemical degradation of epoxidized natural rubber using periodic acid: preparation of epoxidized liquid natural rubber. J Appl Polym Sci 95(1):6–15. https://doi.org/10.1002/app.20812
3. Hsu S-h, Tseng H-J, Lin Y-C (2010) The biocompatibility and antibacterial properties of waterborne polyurethane-silver nanocomposites. Biomaterials 31(26):6796–6808. https://doi.org/10.1016/j.biomaterials.2010.05.015
4. Rithesh Raj D, Sudarsanakumar C (2017) Surface plasmon resonance based fiber optic sensor for the detection of cysteine using diosmin capped silver nanoparticles. Sens Actuators A Phys 253:41–48. https://doi.org/10.1016/j.sna.2016.11.019

5. Dong C, Zhang X, Cai H, Cao C, Zhou K, Wang X, Xiao X (2016) Synthesis of stearic acid-stabilized silver nanoparticles in aqueous solution. Adv Powder Technol 27(6):2416–2423. https://doi.org/10.1016/j.apt.2016.08.018
6. Medici S, Peana M, Nurchi VM, Lachowicz JI, Crisponi G, Zoroddu MA (2015) Noble metals in medicine: latest advances. Coord Chem Rev 284:329–350. https://doi.org/10.1016/j.ccr.2014.-08.002
7. Zhang X, Xiao G, Wang Y, Zhao Y, Su H, Tan T (2017) Preparation of chitosan-TiO_2 composite film with efficient antimicrobial activities under visible light for food packaging applications. Carbohyd Polym 169:101–107. https://doi.org/10.1016/j.carbpol.2017.03.073
8. Dos Santos CA, Seckler MM, Ingle AP, Gupta I, Galdiero S, Galdiero M, Gade A, Rai M (2014) Silver nanoparticles: therapeutical uses, toxicity, and safety issues. J Pharm Sci 103(7):1931–1944. https://doi.org/10.1002/jps.24001
9. Levi-Polyachenko N, Jacob R, Day C, Kuthirummal N (2016) Chitosan wound dressing with hexagonal silver nanoparticles for hyperthermia and enhanced delivery of small molecules. Colloids Surf B Biointerfaces 142:315–324. https://doi.org/10.1016/j.colsurfb.2016.-02.038
10. Macocinschi D, Filip D, Zaltariov MF, Varganici CD (2015) Thermal and hydrolytic stability of silver nanoparticle polyurethane biocomposites for medical applications. Polym Degrad Stab 121:238–246. https://doi.org/10.1016/j.polymdegradstab.2015.09.017
11. Rausch KW, Sayigh AAR (1965) Structure property relationships in polyurethane elastomers prepared by one-step reaction. I&EC Product Res Dev 4(2):92–98. https://doi.org/10.1021/i360014a008
12. Kébir N, Campistron I, Laguerre A, Pilard JF, Bunel C, Jouenne T (2007) Use of telechelic cis-1,4-polyisoprene cationomers in the synthesis of antibacterial ionic polyurethanes and copolyurethanes bearing ammonium groups. Biomaterials 28(29):4200–4208. https://doi.org/10.1016/j.biomaterials.2007.06.006
13. Ranoszek-Soliwoda K, Tomaszewska E, Socha E, Krzyczmonik P, Ignaczak A, Orlowski P, Krzyzowska M, Celichowski G, Grobelny J (2017) The role of tannic acid and sodium citrate in the synthesis of silver nanoparticles. J Nanopart Res 19(8):273. https://doi.org/10.1007/s11051-017-3973-9
14. Zhu Q, Li X, Fan Z, Xu Y, Niu H, Li C, Dang Y, Huang Z, Wang Y, Guan J (2018) Biomimetic polyurethane/TiO_2 nanocomposite scaffolds capable of promoting biomineralization and mesenchymal stem cell proliferation. Mater Sci Eng C Mater Biol Appl 85:79–87. https://doi.org/10.1016/j.msec.2017.12.008
15. da Silva VD, dos Santos LM, Subda S, Ligabue R, Seferin M, Carone C, Einloft S (2013) Synthesis and characterization of polyurethane/titanium dioxide nanocomposites obtained by in situ polymerization. Polym Bull 70:1819–1833. https://doi.org/10.1007/s00289-013-0927-y
16. Al-Naamani L, Dobretsov S, Dutta J (2016) Chitosan-zinc oxide nanoparticle composite coating for active food packaging applications. Innov Food Sci Emerg Technol 38:231–237. https://doi.org/10.1016/j.ifset.2016.10.010
17. Nayak V, Jyothi MS, Balakrishna RG, Padaki M, Ismail AF (2015) Preparation and characterization of chitosan thin films on mixed-matrix membranes for complete removal of chromium. ChemistryOpen 4(3):278–287. https://doi.org/10.1002/open.201402133
18. Zeytuncu B, Morcali MH (2015) Fabrication and characterization of antibacterial polyurethane acrylate-based materials. Mater Res 18:867–872. https://doi.org/10.1590/1516-1439.026515
19. Chung Y-C, Jo SH, Kim HY, Chun BC (2016) Characterization and effect of covalently grafted benzoic acid on the low temperature flexibility and water vapor permeability of a polyurethane copolymer. Polym Plast Technol Eng 55(4):356–367. https://doi.org/10.1080/03602559.2015.-1098678
20. Shahbazi M, Rajabzadeh G, Ahmadi SJ (2017) Characterization of nanocomposite film based on chitosan intercalated in clay platelets by electron beam irradiation. Carbohyd Polym 157:226–235. https://doi.org/10.1016/j.carbpol.2016.09.018
21. D'Orazio L, Grippo A (2015) A water dispersed titanium dioxide/poly-(carbonate urethane) nanocomposite for protecting cultural heritage: preparation and properties. Prog Org Coat 79:1–7. https://doi.org/10.1016/j.porgcoat.2014.09.017
22. Rzeszutek K, Chow A (1998) An investigation into the sorption of benzoic acids by polyurethane membrane. Talanta 47(3):697–709. https://doi.org/10.1016/S0039-9140(98)00115-5
23. Chen JH, Wei J, Chang CY, Laiw RF, Lee YD (1998) Studies on segmented polyether urethane for biomedical application: effects of composition and hard segment content on biocompatibility. J Biomed Mater Res Off J Soc Biomater Jpn Soc Biomater Aust Soc Biomater 41(4):633–648. https://doi.org/10.1002/(SICI)-1097-4636(19980915)41:4%3C633:AIDBM

24. Wang H, Yu J, Fang H, Wei H, Wang X, Ding Y (2018) Largely improved mechanical properties of a biodegradable polyurethane elastomer via polylactide stereocomplexation. Polymer 137:1–12. https://doi.org/10.1016/j.poly-mer.2017.12.067
25. Petrović ZS, Zavargo Z, Flyn JH, Macknight WJ (1994) Thermal degradation of segmented polyurethanes. J Appl Polym Sci 51(6):1087–1095. https://doi.org/10.1002/app.1994.070510615
26. Jiao L, Xiao H, Wang Q, Sun J (2013) Thermal degradation characteristics of rigid polyurethane foam and the volatile products analysis with TG-FTIR-MS. Polym Degrad Stab 98(12):2687–2696. https://doi.org/10.1016/j.polymdegradstab.2013.09.032
27. Rivière L, Caussé N, Lonjon A, Dantras É, Lacabanne C (2016) Specific heat capacity and thermal conductivity of peek/ag nanoparticles composites determined by modulated-temperature differential scanning calorimetry. Polym Degrad Stab 127:98–104. https://doi.org/10.1016/j.polymdegradstab.2015.11.015
28. Smith SJ, Stevens R, Liu S, Li G, Navrotsky A, Boerio-Goates J, Woodfield BF (2009) Heat capacities and thermodynamic functions of TiO_2 anatase and rutile: analysis of phase stability. Am Miner 94(2–3):236–243
29. Thongsang S, Vorakhan W, Wimolmala E, Sombatsompop N (2012) Dynamic mechanical analysis and tribological properties of NR vulcanizates with fly ash/precipitated silica hybrid filler. Tribol Int 53:134–141. https://doi.org/10.1016/j.triboint.2012.04.006
30. Abbasi E, Milani M, Fekri Aval S, Kouhi M, Akbarzadeh A, Tayefi Nasrabadi H, Nikasa P, Joo SW, Hanifehpour Y, Nejati-Koshki K (2016) Silver nanoparticles: synthesis methods, bio-applications and properties. Crit Rev Microbiol 42(2):173–180. https://doi.org/10.3109/-1040841X.2014.912200
31. Willey JM, Sherwood LM, Woolverton CJ (2008) Prescott, Harley and Klein's microbiology, 7th edn. McGrawHill Company, New York, p 578